



HAL
open science

Investigating the influence of the operating frequency on the gas phase emitter effect of dysprosium in ceramic metal halide lamps

J Reinelt, M Westermeier, C Ruhrmann, A Bergner, G M J F Luijks, P Awakowicz, J Mentel

► To cite this version:

J Reinelt, M Westermeier, C Ruhrmann, A Bergner, G M J F Luijks, et al.. Investigating the influence of the operating frequency on the gas phase emitter effect of dysprosium in ceramic metal halide lamps. *Journal of Physics D: Applied Physics*, 2011, 44 (22), pp.224006. 10.1088/0022-3727/44/22/224006 . hal-00620592

HAL Id: hal-00620592

<https://hal.science/hal-00620592>

Submitted on 8 Sep 2011

HAL is a multi-disciplinary open access archive for the deposit and dissemination of scientific research documents, whether they are published or not. The documents may come from teaching and research institutions in France or abroad, or from public or private research centers.

L'archive ouverte pluridisciplinaire **HAL**, est destinée au dépôt et à la diffusion de documents scientifiques de niveau recherche, publiés ou non, émanant des établissements d'enseignement et de recherche français ou étrangers, des laboratoires publics ou privés.

Investigating the influence of the operating frequency on the gas phase emitter effect of dysprosium in ceramic metal halide lamps

J Reinelt^{1,2}, M Westermeier^{1,2}, C Ruhrmann¹, A Bergner¹,
G M J F Luijks³, P Awakowicz¹ and J Mentel¹

¹ Ruhr University Bochum, Electrical Engineering and Plasma Technology, D-44780 Bochum, Germany

² Present address: RWE Effizienz GmbH, Freistuhl 7, D-44137 Dortmund, Germany

³ Philips Lighting, GBU HID, P.O.box 80020, 5600JM Eindhoven, The Netherlands

E-mail: juergen.mentel@ruhr-uni-bochum.de

Abstract. The dependence of the gas phase emitter effect of Dy on a variation of the operating frequency between some Hz and 2 kHz is investigated in a HID lamp. The buffer gas of the lamp consisting of Ar , Kr and predominantly Hg is seeded with DyI_3 , its burner vessel is formed from transparent YAG material. Phase and spatial resolved emission spectroscopy in front of the lamp electrode and pyrometric temperature measurements along the tungsten electrode are performed with a spectroscopic set up. Dy atom and ion densities in front of the electrode are deduced from absolute intensities of optically thin Dy lines and a plasma temperature, derived from the absolute intensity of mercury lines. Phase resolved values of the electrode tip temperature T_{tip} and input power P_{in} are obtained from temperature distributions along the electrode. Distinctly higher Dy ion and atom densities are measured in front of the electrode within the cathodic phase. With increasing operating frequency a reduction of both, atoms and ions, is observed in front of the cathode. In contrast, an increase of the ion density in front of the anode is seen. Moreover, the Dy ion density is drastically reduced by an additional seeding of the lamp with TII . It is found that an up rating of the Dy ion density is correlated with a decline of T_{tip} and P_{in} . At higher frequencies this effect takes place not only within the cathodic phase but also within the anodic phase. The reduction of the average electrode tip temperature on the order of several hundred Kelvin compared to a YAG lamp with a pure mercury filling is explained by a Dy monolayer on the electrode surface which is sustained by a Dy ion current.

Submitted to: *J. Phys. D: Appl. Phys.*

1. Introduction

Today the most effective point shaped light sources to generate visible light for outdoor applications in the range of k-lumens are high intensity discharge (HID) lamps, e.g. high pressure sodium lamps. They are characterized by a high efficacy on the order of 100 – 150 lm/W, a long life time on the order of 10000 – 25000 h and low costs. In addition white light and a high colour rendering can be achieved with a special version of HID lamps: the metal halide (MH) lamps. In these lamps a buffer gas is seeded together with carefully chosen mixes of metal iodides. They can provide rich emission spectra by which white light with high colour quality can be created. A high metal vapour pressure is favourable for a high colour rendering. It is determined by the lowest value of the temperature on the inner wall of the lamp tube, the so called cold spot temperature. To make the cold spot temperature as high as possible the tubes of MH lamps are preferably made of ceramic material, e.g. translucent alumina. It substitutes fused silica which was used previously since it permits higher wall loadings and higher temperatures. As a result ceramic MH lamps are characterized not only by high efficacies and long life times but also by excellent colour rendering indices on the order of 90. For this reason they are increasingly adopted for indoor applications such as shop lighting.

The high demands on the load capacity of the electrodes are one of the main problems with HID lamps. The tip temperature of electrodes made of pure tungsten may increase up to its melting point, $T = 3695$ K, to supply a sufficiently high current density for a diffuse attachment of the lamp arc on the electrodes [1, 2, 3, 4]. But the electrode temperature can substantially be reduced by lowering the work function of the electrode material making use of the so called emitter effect. It is generated by a dipole layer being formed by a monolayer of electropositive atoms on the tungsten surface. It reduces the potential barrier at the electrode surface for electrons leaving or entering the electrode.

Several techniques may be used to form a dipole layer of electropositive atoms on the hot tungsten electrode.

A thorium monolayer may be generated by doping the tungsten electrodes with ThO_2 by an amount of several percent of the electrode volume [5]. A reduction in the effective work function of HID cathodes was verified by pyrometric measurements of the electrode temperature and by probe measurements of the cathode fall in the model lamp [6, 7, 8]. It was also shown by measurements in the model lamp that doping of a tungsten electrode with ThO_2 does not change the anode temperature. It demonstrates that the effective work function of the thoriated anode is comparable to that of a pure tungsten anode [9, 10].

Another approach to forming a dipole layer is to deposit emitter material, e.g. a

Ba-compound (Ba_2CaWO_6 or $Ba_3Y_2WO_9$) within the interspaces of a closely wound tungsten coil at some distance from the electrode tip. When the electrode is heated up the compound is dissociated and the *Ba* emitter diffuses along the electrode surface to the tip [5], a theory, which was recently confirmed by measurements [11].

A quite versatile approach is the deposition of an atomic monolayer on the electrode surface from the gas phase being called “gas phase emitter effect” [12]. A reduction of the work function by a sodium monolayer on the cathode and anode of a high pressure sodium (HPS) lamp could be demonstrated if appropriate lamp parameters were chosen [13, 14]. A monolayer can be realized with a large variety of elements by adding appropriate metal iodides to the lamp filling. They are vaporized and dissociated during lamp operation so that a partial pressure of metal vapour is formed within the lamp tube. A gas phase emitter effect induced by a ThI_4 additive was demonstrated already many years ago in a high pressure mercury lamp operated with an ac current [15]. But it is not clear whether the emitter effect is limited to the cathodic half period or is also effective within the anodic half period.

A gas phase emitter effect can also be realized if a HID metal halide lamp is seeded with rare earth iodides. A detailed investigation of this effect in a ceramic metal halide lamp operated with a dc current in a mercury atmosphere seeded with different mixtures of NaI , TlI and DyI_3 is given in [12]. A transparent ceramic YAG tube was used to allow electrode temperature measurements. A distinct reduction in the work function at the cathode was demonstrated by a measured drastic reduction of the cathode temperature. At the anode a minor or even doubtful emitter effect was found by measurements of the electrode tip temperature. If the lamp is operated with a switched dc current an increase of the average electrode tip temperature T_{tip} within the cathodic phase was found by reason of anode heating during the preceding anodic half period. However, the averaged temperature remains below the value for a lamp with a pure mercury filling [16, 17]. By spectroscopic measurements of the *Dy* atom and ion density it was shown that a decrease of the electrode temperature is correlated with an increased *Dy* atom and ion density in front of the electrode [16].

This observation has brought up the idea that the *Dy* layer on the electrode is mainly formed by a *Dy* ion current towards the electrode during the cathodic phase. A generation of the emitter effect by an ion current may explain why an additional seeding of the YAG lamp with sodium seems to hamper the emitter effect of *Dy* [16]. In this case predominantly a *Na* ion current in front of the cathode is formed since the ionisation energy of *Na* ($E_i = 5.139$ eV) is lower and its mass ($A_r = 23$) smaller than that of *Dy* ($E_i = 5.93$ eV, $A_r = 162.5$). But the adsorption energy E_a of *Na* on a tungsten surface ($E_a = 2.33$ eV) is distinctly smaller than that of *Dy* ($E_a = 4.97$ eV) so that it is, different to *Dy*, less appropriate to form a stable monolayer on a hot electrode within a MH lamp [18, 19, 20].

The importance of an ion current of the emitter material to the cathode is also indicated by an advancement of the spot attachment with an increasing Dy density [12, 16, 21]. The shape of the spot induced by a high Dy density differs from the spot mode investigated in great detail in [1, 3, 22, 23, 24, 25, 26]. The spot attachment induced by the gas phase emitter effect should therefore be called “emitter spot”. The statement in [27] that the emitter effect favours the formation of a diffuse mode obviously does not apply to the emitter spot.

The behaviour of tungsten electrodes for HID lamps was investigated recently in the so called Bochum model lamp filled with argon [6] in dependence on the operating frequency being varied between 10 Hz and 10 kHz [28]. The Bochum model lamp is formed by a quartz tube, sealed vacuum-tight by two metallic end pieces with feed-throughs containing movable holders for the tungsten electrodes. The measuring results have shown that the cathodic phase becomes more and more dominant with increasing operating frequency. It was found that with increasing operating frequency the electrode temperature approaches the value of the cathode at dc operation, while the influence of the anodic phase is pushed back. The same may happen in MH lamps, in which the gas phase emitter effect is heavily dependent on the electrode polarity.

To check this speculation the electrodes of YAG lamps and the plasma in front of them are investigated in dependence on the operating frequency being varied between 1 Hz and 2 kHz. Phase resolved pyrometric measurements of the electrode temperature and phase resolved measurements of the Dy atom and ion density are accomplished by emission spectroscopy. Appropriate measuring methods are already given in previous papers [16, 28] so that only a short sketch will be given. YAG lamps with different fillings and electrodes with different diameters are operated with a switched dc current of constant amplitude but different operating frequencies. Initially, as a reference, phase resolved electrode tip temperatures and plasma temperatures in front of the electrode are given for a YAG lamp with a pure mercury filling. The plasma temperatures are deduced from the absolute intensity of mercury lines. In a next step YAG lamps, in which the buffer gas mercury is only seeded with DyI_3 , are investigated for electrodes with different diameters. To clarify the role of thallium in MH lamps some measurements of YAG lamps are given, which are seeded with a mixture of TlI and DyI_3 . The major part of this investigation extends measurements to higher frequencies which were already made at low operating frequencies [16]. The paper is to a large extent an excerpt of Reinelt’s PhD thesis [29].

2. Experimental setup

2.1. YAG lamp

The HID lamps under investigation have a special research design being given in detail in [12]. A burner vessel with an ovoid shape is formed from yttrium-alumina-garnet (YAG), a transparent material, which allows optical observation. Tungsten rod electrodes are mounted on a *Mo* feedthrough for ceramic lamps and sealed in the lamps using a sealing ceramic. The electrodes have a diameter of $d = 360, 450$ and $500 \mu\text{m}$ and an interelectrode spacing of $g = 7 \text{ mm}$. The electrodes extend 5 mm into the tube, their total length is $20\text{-}25 \text{ mm}$. The burner is enveloped by an outer glass bulb furnished with a lamp base. The lamp is filled with an argon-krypton mixture as buffer gas at a pressure of $p = 30 \text{ kPa}$ for lamp ignition and in addition with an amount of mercury that produces an unsaturated mercury background pressure of $p = 2 \text{ MPa}$ [12]. Some lamps are seeded with DyI_3 , another one with a mixture of DyI_3 and TlI . For comparison also lamps without any salt additive are investigated. The properties of lamps for which measurements are presented are listed in table 1. The lamps are designed for an effective electrical power of $P_{el} = 70 \text{ W}$. The lamps are operated in a vertical position with the cold spot and the salt pool associated with it on the lower end of the lamp. The optical measurements are performed at the upper electrode since at the lower electrode the transparency of the tube wall is affected by the liquid salt pool.

Lamp type	Electrode diameter (μm)	Electrode length (mm)	Hg (mg)	Total salt (mg)	Tl (mol%)	Dy (mol%)
Hg	$d = 360$	$l = 5$	6	0	0	0
D	$d = 360$	$l = 5$	6	1	0	100
D	$d = 450$	$l = 5$	6	1	0	100
D	$d = 500$	$l = 5$	6	1	0	100
TD	$d = 450$	$l = 5$	6	2	50	50

Table 1. Properties of the lamps investigated in this work

The YAG lamp is operated with a current source (Feucht Elektronik DCU/I 2250-30) being controlled by the output voltage of a signal generator. It is able to provide dc, ac, pulsed or transient currents of arbitrary waveform up to frequency of 30 kHz , a current amplitude of several amps and a maximum open-circuit voltage of 400 V .

Standing acoustic oscillations may occur in MH lamps within various frequency regions. The YAG lamps being investigated here are undisturbed by acoustic resonances in the following frequency bands:

$$f \leq 3500 \text{ Hz}$$

$$f = 23.2 \text{ kHz} \tag{1}$$

$$f \geq 300 \text{ kHz}$$

2.2. Measuring system for phase resolved emission spectroscopy

Almost the same spectroscopic measuring system is used for phase resolved measurements of the electrode temperature and of the particle densities in front of the electrode. Only some minor modifications are needed. The experimental setup was already described in [16, 25], so that a sketch will be sufficient here.

The spectrograph in use is a 250 mm apparatus from Chromex with an aperture ratio of $f/4.0$. A grating is used mostly with a line density of 1200 mm^{-1} . The entrance slit is adjusted for pyrometric measurements to a width of $100 \mu\text{m}$ and in the case of spectroscopic measurements to $25 \mu\text{m}$. To record the emission of the lamp by the spectrograph an optical imaging system is mounted in between. A telecentric imaging system consisting of two achromats projects an image of the lamp onto the entrance plane of the spectrograph with a magnification of $M = 1$. A Dove prism between the two achromats is used to adjust either the image of the electrode parallel or the discharge axis perpendicular to the vertical entrance slit of the spectrograph.

The output of the spectrograph is recorded with a CCD camera SENSICAM QE from PCO mounted in the image plane of it. The camera resolution along the entrance slit is 1376 pixel and along the wavelength axis 1040 pixel. The pixel size amounts to $6.45 \mu\text{m} \times 6.45 \mu\text{m}$. It determines the spatial resolution along the entrance slit of the spectrograph. The camera offers the possibility of an internal binning summing up the counts of a defined number of adjacent pixel. The dynamic range of the camera is 14 bits which implies a maximum count rate of 4096 counts per pixel. The exposure time of the camera t_{exp} can be varied between 500 ns and 3600 s. The CCD chip of the camera is sensitive within the wavelength interval from 280 to 1100 nm. A calibration of the optical system in absolute values of radiance is needed for the measurements at the electrode and at the plasma. For this purpose a tungsten ribbon lamp (Wi17g3 from OSRAM) with a known radiance in dependence on wavelength for a specified current is positioned on the same place as the lamp under investigation.

The temporal resolution of the camera is limited by the read out time of the CCD chip, which amounts approximately to 90 ms. This means that for operating frequencies above $f > 5 \text{ Hz}$ not more than one measurement within one half period can be made. Therefore repeated phase resolved measurements are needed to get information about the time-evolution of phenomena of interest within the half period. The substitution of a temporal by a phase resolution does not raise a problem as long as the lamp operation is really periodic. In this case only a reproducible periodical trigger signal is required

Investigating the influence of the operating frequency on the gas phase emitter effect of Dy7
as a starting point for a series of successively phase delayed exposures.

The delay time of the current source, which is realized by an electronic device, varies too much in dependence on the operating parameters that the “sync” output of the signal generator, by which the current source is controlled, is suitable to provide an appropriate trigger pulse. Thus the reference phase has to be generated on the output side of the amplifier. The current zero crossing is inapplicable since the current may not rise fast enough after current zero crossing to be able to generate a well defined trigger pulse. Therefore the trigger signal is deduced from the voltage zero crossing of the lamp [24]. To trigger the camera only the rising edge of the voltage signal is used. The uncertainty of the trigger pulse does not exceed $2 \mu\text{s}$. To take pictures at different phase angles φ a delay generator (STANFORD RESEARCH SYSTEM DG 535) is used to shift the trigger signal from voltage zero crossing. A block diagram of the trigger set up is already given in [25].

3. Pyrometric electrode temperature measurement

It is favorable for the pyrometric measurements to use a segment of the spectrum emitted by the electrode, which is as far as possible in the infrared region but still in the sensitivity range of the CCD camera. Furthermore, the plasma radiation emitted by the YAG lamps should be negligible compared to the emission of the electrode surface. A suitable wavelength for temperature measurements of the electrodes in the YAG lamps is $\lambda = 718 \text{ nm}$. An edge filter with an edge wavelength $\lambda_{edge} = 600 \text{ nm}$ is used to suppress all radiation with a wavelength below λ_{edge} . It prevents a falsification of the measurement by the second order spectrum produced by the grating emitted at $\lambda_{meas}/2$. The integral transmission Tr of the YAG tube and of the outer glass bulb which has to be taken into account amounts to $Tr \approx 72\%$ at $\lambda_{meas} = 718 \text{ nm}$.

A spatial profile of the spectral radiance I_{el} of the electrode at $\lambda = 718 \text{ nm}$ along the electrode length within the tube is recorded by a single measurement at a selected phase angle φ . A grey body radiator is assumed to determine axial temperature profiles $T(z, \varphi)$ from the measured radiances $I_{el}(z, \varphi)$. The spectral radiance of the grey body $I_{gb}(\lambda, T)$ is given by Planck’s law and by temperature and wavelength dependent spectral emissivity $\epsilon(\lambda, T) < 1$. An inspection of literature [30] and a comparison between measurements and simulation ([3] figure 14) showed that the spectral emissivities of de Vos [31] are the most trustable ones. Spatial profiles $T(z, \varphi)$ are determined comparing measured values $I_{el}(z, \varphi)$ with $I_{gb}(T, \lambda = 718 \text{ nm})$ calculated in dependence on T . The accuracy of the temperature measurements especially in the vicinity of the electrode tip is mainly affected by questionable values of ϵ . They are in general exaggerated in an undefined manner by an enhanced surface roughness being produced by the arc attachment at the electrode tip. The exaggerated values of ϵ increase the radiance at the electrode tip so that the comparison with the calculated values of $I_{gb}(T)$ delivers too

high temperature values at the electrode tip T_{tip} .

Reliable values of T_{tip} were obtained in [6] for electrodes operated with a dc current by matching measured temperature distributions $T(z)$ within a region of confidence between a lower temperature limit T_l and an upper temperature limit $T_{up} < T_{tip}$ by a least square fit procedure to numerical solutions of the one dimensional heat balance of the electrode. The electrode tip temperature T_{tip} and the total power input into the electrode P_{in} were determined by extrapolating the solutions up to the electrode tip. But it was shown in [28] that the method becomes questionable if in the case of an ac operation the heat capacity of the electrode has an influence on the temperature distribution. A distinct variation of the temperature with φ occurs only in the vicinity of the electrode tip, but disappears with increasing distance from the tip [25]. Its extension is given by the penetration depth of a sinusoidal modulation of the temperature at the electrode tip

$$\lambda_{pen} = \left(\frac{\kappa}{\rho_M c_p 2\pi f} \right)^{1/2} \quad (2)$$

where $\kappa(T)$ is the thermal conductivity of tungsten in dependence on temperature, ρ_M the mass density of tungsten and $c_p(T)$ its heat capacity per unit mass. A comprehensive presentation of the data is given in [30]. λ_{pen} decreases with $f^{-1/2}$ and is already less than 1 mm for $f = 10$ Hz and $T = 3000$ K. This means that $T_{tip}(\varphi)$ can, different to [6], only be determined with an appropriate phase resolution if the temperature distribution in the vicinity of the electrode tip can be taken into account.

For this purpose the time dependent heat balance of the electrode was considered in [28]. A rotational symmetric electrode temperature distribution is assumed as it is realized by a diffuse attachment of an arc on the electrode. Additionally the r -dependence of T along the electrode rod is neglected. A thin disk of the electrode of thickness dz in a distance z from the electrode tip and a change of the phase angle $d\varphi$ is considered to calculate the power balance of the electrode in dependence on time/phase. Since during the exposure time $t_e = \omega^{-1}\varphi_e$ of the camera $\left(\frac{\partial T}{\partial t}\right)_{t_e} = \omega \left(\frac{\partial T}{\partial \varphi}\right)_{\varphi_e}$ is almost constant, the spatial derivative $\partial T/\partial z$ can be substituted by the total derivative dT/dz . Thus, the heat balance of the electrode disk can be written as:

$$r_E^2 \pi \frac{d}{dz} \left(\kappa(T) \frac{dT}{dz} \right) = -2\pi r_E q_E(T) + 2\pi r_E \epsilon_{tot} \sigma_{SB} T^4 + r_E^2 \pi \frac{\kappa}{\lambda_{pen}^2} \left(\frac{\partial T}{\partial \varphi} \right)_{\varphi_e}, \quad (3)$$

where r_E is the electrode radius, $q_E(T)$ the power input per unit area from the plasma into the cylinder barrel of the rod, ϵ_{tot} the total emissivity of tungsten and σ_{SB} the Stefan-Boltzmann constant. Data for ϵ_{tot} are given in [30]. An analytic solution of the differential equation was given in [28]:

$$z(T) =$$

Investigating the influence of the operating frequency on the gas phase emitter effect of Dy9

$$\int_{T'=T}^{T_{tip}} \frac{\kappa(T')dT'}{\left[\left(\kappa(T') \frac{dT}{dz} \right)_{T_{tip}}^2 + \frac{4}{r_E} \int_{\tau=T'}^{T_{tip}} q_E \kappa d\tau - \frac{4}{r_E} \int_{\tau=T'}^{T_{tip}} \epsilon_{tot} \sigma_{SB} \tau^4 \kappa d\tau - 2 \int_{\tau=T'}^{T_{tip}} \frac{\kappa^2}{\lambda_{pen}^2} \left(\frac{\partial \tau}{\partial \varphi} \right)_{\varphi_e} d\tau \right]^{1/2}} \quad (4)$$

$z = 0$ is the position of the end face of the electrode, the integration constants are $T(z = 0) = T_{tip}$ and $(\kappa dT/dz)_{T_{tip}}$.

According to [28] the first and second term within the square root under the fraction bar on the right hand side of eq. 4 can be written as:

$$\left(\kappa \frac{dT}{dz} \right)_{T_{tip}}^2 + \frac{4}{r_E} \int_{\tau=T}^{T_{tip}} q_E(\tau) \kappa d\tau = \frac{(P_{in} - P_r)^2 - P_c^2}{(\pi r_E^2)^2} \quad (5)$$

P_{in} is the total power input into the electrode and P_r the radiant power, which is emitted from the end face of the electrode. The quantity

$$P_c = 2\pi r_E \int_0^z q_E dz, \quad \text{with } q_E \neq 0 \text{ for } z < r_E \quad (6)$$

represents the power input into the cylinder barrel of the rod, which can be neglected as was shown in [28] if the major part of the power is supplied into the end face of the electrode. For $P_c^2 / (P_{in} - P_r)^2 \ll 1$ the temperature distribution along the electrode can be written as:

$$z(T) \approx \int_{T'=T}^{T_{tip}} \frac{\kappa(T')dT'}{\left[\left(\frac{P_{in} - P_r}{\pi r_E^2} \right)^2 - \frac{4}{r_E} \int_{\tau=T'}^{T_{tip}} \epsilon_{tot} \sigma_{SB} \tau^4 \kappa d\tau - 2 \int_{\tau=T'}^{T_{tip}} \frac{\kappa^2}{\lambda_{pen}^2} \left(\frac{\partial \tau}{\partial \varphi} \right)_{\varphi_e} d\tau \right]^{1/2}} \quad (7)$$

The integral can be used to simulate a temperature distribution $z_{sim}(T)$ if measured values for $(\partial T / \partial \varphi)_{\varphi_e}$ and estimated values for T_{tip} and $P_{in} - P_r$ are inserted.

Measured values $z_{meas}(T)$ between a lower temperature T_l and an upper temperature T_{up} will be used to determine appropriate values of T_{tip} and P_{in} by searching the minimum of

$$f(P_{in}, T_{tip}) = \int_{T_l}^{T_{up}} [z_{meas} - z_{sim}]^2 dT. \quad (8)$$

Compared to [6] the new procedure offers the possibility to take into account the variation $(\partial T / \partial \varphi)_{\varphi_e}$ in the vicinity of the electrode tip. But the fundamental problem with the exaggerated temperature at the electrode tip and the limited penetration depth λ_{pen} is not really removed. On the other hand the amplitude modulation of $T_{tip}(\varphi)$ in dependence on the phase modulation of the power input $P_{in}(\varphi)$:

$$\Delta T_{tip}(\varphi) \propto \frac{\Delta P_{in}(\varphi)}{\rho_M c_p \pi r_E^2 \lambda_{pen} 2\pi f} \quad (9)$$

decreases as λ_{pen} with $f^{-1/2}$, where $\pi r_E^2 \lambda_{pen}$ represents the volume at the electrode tip in which a temperature variation takes place. It mitigates the problem with the modulation of T_{tip} with increasing frequency.

In [28] it was shown that the phase resolved experimental determination of T_{tip} is afflicted with an error on the order of $\Delta T_{tip} \approx 50$ K and P_{in} with an error on the order of 10 %. Errors on this order of magnitude have to be taken into account appraising the measurements of $T_{tip}(\varphi)$ and $P_{in}(\varphi)$ given below.

4. Spectroscopic particle density measurement

Phase resolved measurements of the *Dy* atom and ion density are carried out by the same measuring procedure as in [16]. Only the operating frequencies are extended up to 2 kHz. In addition the lamp filling is modified in part. Different to the pyrometric measurements the image of the vertically operated lamp is rotated through 90° by the Dove prism around the axis of vision so that it is oriented perpendicular to the slit of the spectrograph. The slit captures the emission of a discharge cross section at a distance of 125 μm from the electrode tip.

A LTE plasma with an equal temperature for all species, which represents the local plasma temperature T , and a Boltzmann-population of excited states is assumed by reason of the high filling gas pressure. The assumption was confirmed recently by a combination of absorption and emission spectroscopy at YAG lamps [11, 32].

In a first step the plasma temperature is determined using the emission of two overlapping mercury lines [33]. At first the absolute intensity of the two lines at $\lambda_1 = 576.96$ nm and $\lambda_2 = 579.07$ nm of atomic mercury is measured in dependence on the distance from the discharge axis. This results in a more or less axial symmetric distribution of the radiance of the two lines being integrated over a wavelength interval, covering the two lines, calibrated in absolute units. The sum of the emission coefficients of the two lines $\epsilon_{ul} = \epsilon_1 + \epsilon_2$ is determined in dependence on the distance r from the discharge axis by an inverse Abel transformation. The summed up emission coefficients ϵ_{ul} are related to the plasma temperature according to:

$$\epsilon_{ul} = \frac{hc_0}{4\pi} \frac{p_0}{k_B T} \frac{1}{Q_{Hg}(T)} \left[\frac{g_1 A_{1l}}{\lambda_1} \exp\left(-\frac{E_1}{k_B T}\right) + \frac{g_2 A_{2l}}{\lambda_2} \exp\left(-\frac{E_2}{k_B T}\right) \right] \quad (10)$$

where p_0 is the pressure of the mercury vapour, $Q_{Hg}(T)$ the partition function of Hg atoms, given by $Q_{Hg}(T < 7000 \text{ K}) \approx 1$, A_1 and A_2 the transition probabilities of the two lines, g_1 and g_2 the statistical weights and E_1 and E_2 the excitation energies of the upper line levels. Numerical values of the line data needed in eq. 10 are given in table 2. The other symbols in eq. 10 have the usual meaning. Eq. 10 is used to determine the plasma temperature $T(r)$ from the measured results $\epsilon_{ul}(r)$.

$\lambda_1 = 576.96 \text{ nm}$	$\lambda_2 = 579.07 \text{ nm}$
$g_1 A_1 = 1.18 \cdot 10^8 \text{ s}^{-1}$	$g_2 A_2 = 1.07 \cdot 10^8 \text{ s}^{-1}$
$E_1 = 8.849 \text{ eV}$	$E_2 = 8.842 \text{ eV}$

Table 2. Spectroscopic data for the calculation of mercury temperature from Hg-line intensities

The density N_a of the *Dy* atoms and N_i of the *Dy* ions are obtained from the spectroscopically measured local emission coefficient ϵ_{ul}^a of an atomic line and ϵ_{ul}^i of an ionic line emitted by optical transitions between an upper level u and a lower level l .

An appropriate atomic line is the 695.81 nm line, a resonance line which is nevertheless optically thin by reason of the low transition probability. Comparisons of line profiles in [16] and of plasma temperatures measured with mercury lines and with *Dy* lines, respectively, in [32] have confirmed that the 695.81 nm line is really optically thin. A suitable *Dy* ion line with sufficiently high intensity is the 394.46 nm line. The specific constants of the two lines are given in table 3 [34].

$\lambda_a = 695.81 \text{ nm}$	$\lambda_i = 394.46 \text{ nm}$
$g_a = 15$	$g_i = 18$
$A_a = 8.766 \cdot 10^4 \text{ s}^{-1}$	$A_i = 2.550 \cdot 10^7 \text{ s}^{-1}$
$E_a = 1.7815 \text{ eV}$	$E_i = 3.1424 \text{ eV}$

Table 3. Spectroscopic data for the calculation of dysprosium atom and ion densities from Dy-atom- and ion-line intensities

The emission coefficients ϵ_{ul}^a and ϵ_{ul}^i are the result of an inverse Abel transformation of the lateral radiance distribution of the atomic line at $\lambda_a = 695.81 \text{ nm}$ and of the ionic line at $\lambda_i = 394.46 \text{ nm}$, being determined in absolute units in front of the electrode. Both emission coefficients are related to the population densities of the upper line levels N_u according to:

$$\epsilon_{ul} = \frac{1}{4\pi} N_u A_{ul} \frac{hc_0}{\lambda_{ul}} . \quad (11)$$

The densities of the upper line levels N_u are related to those of the total densities N according to:

$$N = N_u \frac{Q(T)}{g_u} \exp\left(\frac{E_u}{k_B T}\right) \quad (12)$$

where $Q(T)$ is the partition function of the particle species being considered, g_u the statistical weight and E_u the excitation energy of the upper level. With eq. 11 the

population density of the upper emitting atomic state $N_{a,u}$ and ionic state $N_{i,u}$ are calculated and in a second step with eq. 12 the total atom density N_a and total ion density N_i .

The error margins of N_a and N_i may be estimated making use of the logarithmic derivative of eq. 12:

$$\left| \frac{\Delta N}{N} \right| = \left| \frac{\Delta N_u}{N_u} \right| + \left| \frac{E_u}{k_B T} \frac{\Delta T}{T} \right| + \left| \frac{\partial \ln Q}{\partial \ln T} \frac{\Delta T}{T} \right| \quad (13)$$

The error margin of N_u is composed of the error margin of ϵ_{ul} and that of A_{ul} :

$$\left| \frac{\Delta N}{N} \right| = \left| \frac{\Delta \epsilon_{ul}}{\epsilon_{ul}} \right| + \left| \frac{\Delta A_{ul}}{A_{ul}} \right| \quad (14)$$

The emission coefficients ϵ_{ul} are afflicted at least with an error of 20 %. It is mainly caused by the inverse Abel transformation, which reacts, particularly on the axis, quite sensitively on deviations from symmetry of the lateral distribution of the line intensity. It has also to be taken into account that the transmission of the lamp tube may be reduced during lamp operation. Additionally the SNR especially of the 394.46 nm line becomes low, if for high operating frequencies short exposure times are required. Besides the knowledge of the transition probability A_{ul} is correct not better than 10 %. Another important error source is according to eq. 13 the uncertainty of the plasma temperature $\Delta T/T$ by reason of the multiplier $E_u/k_B T$. The plasma temperature in front of the electrode is $T \approx 7000$ K [16], with an error margin of about 4 %. The multiplier is $E_{a,u}/k_B T \approx 3$ for the atoms N_a and $E_{i,u}/k_B T \approx 5$ for the ions N_i . The multiplier of the third term in eq. 13 is roughly $\partial \ln Q / \partial \ln T \approx 1$ so that its contribution to the total error margin is minor.

The resulting error margins are: $|\Delta N_a/N_a| \cdot 100 \geq 40$ % and $|\Delta N_i/N_i| \cdot 100 \geq 50$ %. They reveal that the numerical values of the particle densities obtained by the spectroscopic measurements are only in the order of magnitude correct. But the variations in dependence on phase, $\partial N_a / \partial \varphi$ and $\partial N_i / \partial \varphi$, represent a quite reliable information. Subsequently the reported values of T , N_a and N_i are averages over a rotational symmetric cross section with the same diameter as the electrode.

5. Results of measurements at the YAG lamp

Results for the density of *Dy* atoms N_a and *Dy* ions N_i , of the electrode tip temperature T_{tip} and of the input power P_{in} into the electrode are presented in dependence on the phase angle φ . All pyrometric measurements are performed at the upper electrode, all spectroscopic measurements in front of the upper electrode. Measurements are executed at operating frequencies of 1, 10, 25, 50, 100, 250, 500 Hz, 1 and 2 kHz. For frequencies up to 100 Hz measurements are carried out at 20 equidistant phase angles $\varphi_\nu = 0.1\pi\nu$, ($\nu = 1 - 20$) over one period. For $f > 100$ Hz the number of measuring points is individually adjusted to a lower rate so that the SNR can be kept sufficiently high for a

suitable measurement. For $f = 2$ kHz mostly only one measurement within the anodic and cathodic half period was possible. In the subsequent figures the measurements within the anodic half period are presented between $\varphi = 0$ and $\varphi = \pi$, and those within the cathodic half period between $\varphi = \pi$ and $\varphi = 2\pi$.

5.1. YAG lamp with Hg filling only

At first the properties of a YAG lamp operated with a pure mercury vapour atmosphere are investigated in dependence on the operating frequency for comparison with lamps seeded with metal halides. The electrode diameter amounts to $d_E = 0.36$ mm, its extension into the tube to $l_E = 5$ mm. The lamp is operated with a switched dc current with an amplitude of 0.8 A. For this current amplitude the heating of the electrode is higher within the anodic phase than within the cathodic phase at least for dc operation and for ac operation with low commutation frequencies. The formation of a spot mode at the beginning of the cathodic phase is avoided by this choice of parameters [24]. The operating frequencies are $f = 1, 10, 25, 50, 100, 250, 500$ Hz and 1 kHz.

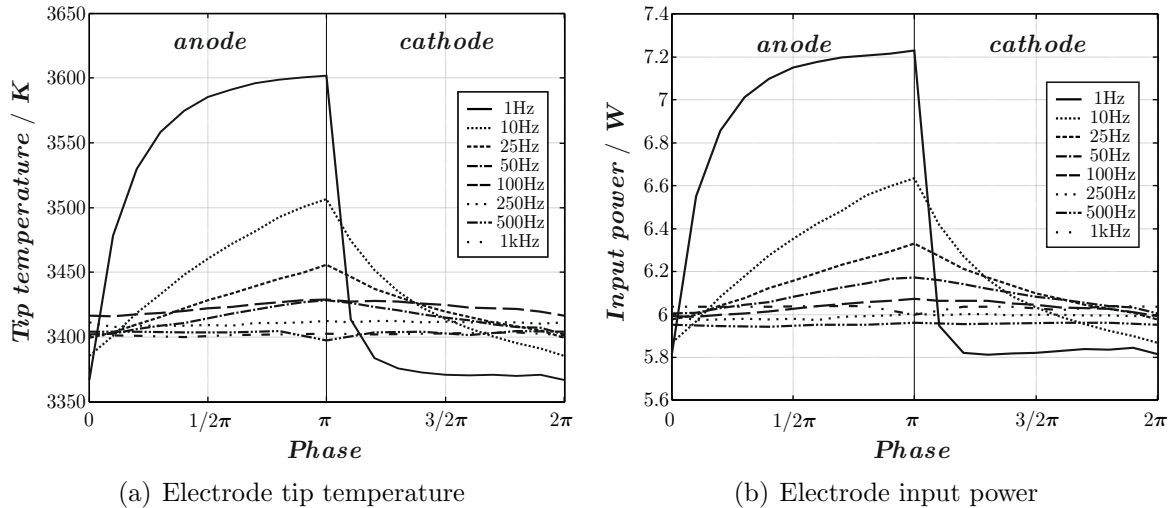


Figure 1. Electrode tip temperature $T_{tip}(\varphi)$ and input power $P_{in}(\varphi)$ over one period for various frequencies. Parameter: Hg, electrode diameter $d_E = 0.36$ mm, electrode length $l_E = 5$ mm, $i = 0.8$ A switched-dc

Figure 1(a) shows the variation of the electrode tip temperature $T_{tip}(\varphi)$ in dependence on the phase angle φ and figure 1(b) the variation of the power input $P_{in}(\varphi)$. Figure 1(a) and 1(b) demonstrate a pronounced reduction of $T_{tip}(\varphi)$ and $P_{in}(\varphi)$ within the anodic phase and a weak lifting of both quantities within the cathodic phase with increasing operating frequency. Small deviations from the general trend e.g. for $f = 100$ Hz are within the error bars. For $f \geq 250$ Hz the differences between the anodic and cathodic phase become almost indistinguishable. The nearly constant magnitude of T_{tip} and P_{in} is only marginally higher than T_{tip} and P_{in} of a dc operated cathode,

which is loaded with the same current amplitude. The results are in general agreement with those obtained by measurements at the model lamp with a pure argon filling [28].

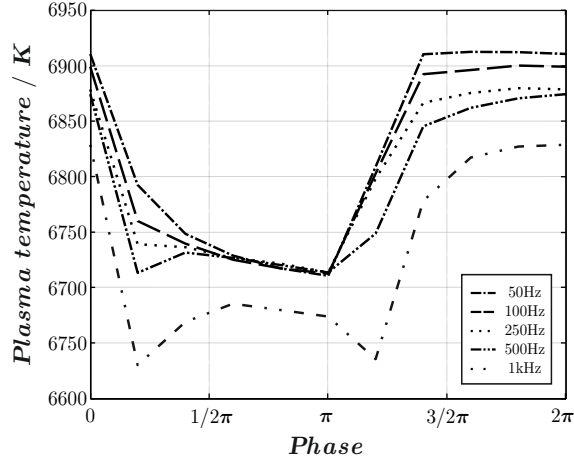


Figure 2. Plasma temperature $T(\varphi)$ over one period for various frequencies measured at a distance of $125 \mu\text{m}$ in front of the electrode surface. Parameter: Hg , electrode diameter $d_E = 0.36 \text{ mm}$, electrode length $l_E = 5 \text{ mm}$, $i = 0.8 \text{ A}$ switched-dc

In figure 2 the variation of the plasma temperature T at a distance $z = 125 \mu\text{m}$ from the electrode tip within a YAG tube is given in dependence on the phase angle φ . The tube parameters are the same as in figure 1, the amplitude of the switched dc current is $i = 0.8 \text{ A}$, the operating frequencies are $f = 50, 100, 250, 500 \text{ Hz}$ and 1 kHz . T is deduced from the measured lateral distribution of the absolute intensities of the two mercury lines at $\lambda_1 = 576.96 \text{ nm}$ and $\lambda_2 = 579.07 \text{ nm}$. The plasma temperature T is approximately 200 K higher within the cathodic phase than within the anodic phase. It reflects the generation of an ion current in front of the cathode, to balance the power consumption by thermionic electron emission of the electrode within the cathodic phase. It decreases with increasing operating frequency namely approximately by 100 K within the cathodic phase and by 50 K within the anodic phase.

5.2. YAG lamp seeded with DyI_3

In a next step YAG lamps with the same design as the mercury lamp but additionally seeded with 1 mg DyI_3 are investigated. In particular the dimension of the electrodes is the same: $d_E = 0.36 \text{ mm}$, $l_E = 5 \text{ mm}$. Results for $N_a(\varphi)$, $N_i(\varphi)$, $T_{tip}(\varphi)$ and $P_{in}(\varphi)$ are given for a lamp which is operated with a switched dc current of $i = 0.8 \text{ A}$. The operating frequencies are $f = 25, 50, 100 \text{ Hz}$ and 2 kHz .

Figure 3(a) and 3(b) show the Dy atom density $N_a(\varphi)$ and the Dy ion density $N_i(\varphi)$, respectively, both versus phase angle φ . The Dy atom density grows for frequencies $f \leq 50 \text{ Hz}$ within the cathodic phase up to $N_a = 10^{22} \text{ m}^{-3}$, which is an order

Investigating the influence of the operating frequency on the gas phase emitter effect of DyI_3

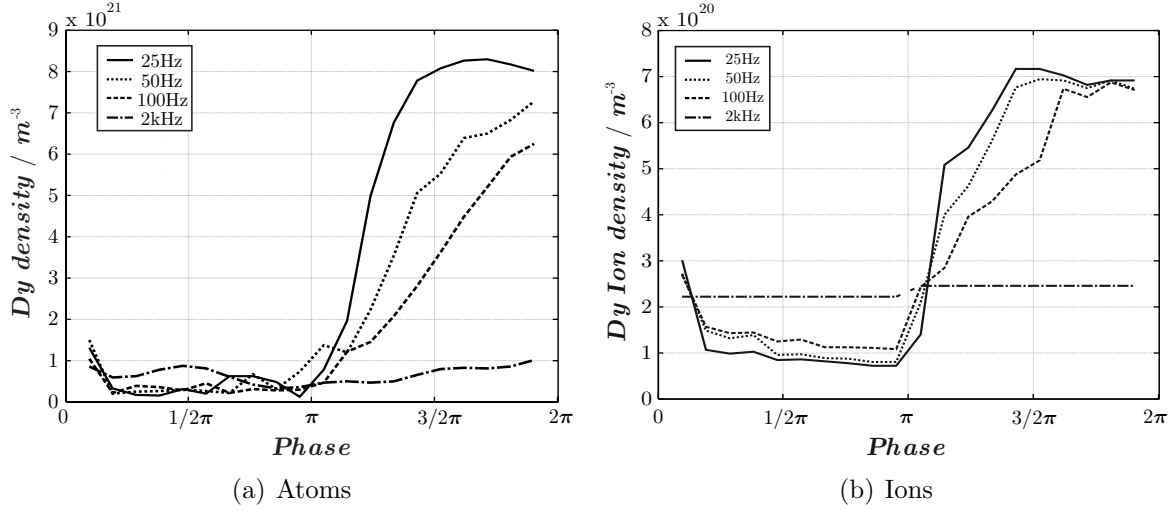


Figure 3. Dysprosium atom density $N_a(\varphi)$ and ion density $N_i(\varphi)$ over one period for various frequencies at a distance of $125 \mu\text{m}$ in front of the electrode. Parameter: DyI_3 , electrode diameter $d_E = 0.36 \text{ mm}$, electrode length $l_E = 5 \text{ mm}$, $i = 0.8 \text{ A}$ switched-dc

of magnitude higher than within the anodic phase. A saturation of N_a occurs approximately after $\tau_a \approx 10 \text{ ms}$. For $f > 50 \text{ Hz}$ the half period is too short to achieve the saturated Dy atom density. As a consequence the maximum value of N_a drops down within the cathodic phase with increasing operating frequency. The Dy ion density N_i rises as well from a value of approximately 10^{20} m^{-3} within the anodic phase to $7 \cdot 10^{20} \text{ m}^{-3}$ within the cathodic phase. A saturation of N_i is already achieved within $\tau_i \approx 5 \text{ ms}$. Therefore the half period becomes too short for $f > 100 \text{ Hz}$ to sustain the modulation of N_i being observed at lower operating frequencies. For $f = 2 \text{ kHz}$ the ion densities within the anodic and cathodic phase have matched by a lifting of N_i within the anodic phase and a lowering of N_i within the cathodic phase.

In figure 4(a) values of N_a within the anodic and cathodic phase averaged over the half period are given in dependence on the operating frequency f and in figure 4(b) the corresponding values of $N_i(f)$. N_a is nearly independent of f within the anodic phase. But within the cathodic phase it decreases monotonically by an order of magnitude from a high value at low operating frequencies down to the value of N_a in front of the anode at higher frequencies. A quite similar behaviour is observed for the Dy ion density N_i . However, different to N_a , the ion density N_i in front of the anode increases at higher frequencies by a factor of approximately two.

The effects of DyI_3 on the electrode tip temperature $T_{tip}(\varphi)$ and on the power input $P_{in}(\varphi)$ are presented in figure 5(a) and in figure 5(b), respectively. A comparison of $T_{tip}(\varphi)$ in figure 1(a) and figure 5(a) clearly demonstrates a reduction of $T_{tip}(\varphi)$ by approximately 400 K for all operating frequencies as a result of the addition of DyI_3 . The reduction of $T_{tip}(\varphi)$ with increasing operating frequency not only within the anodic

Investigating the influence of the operating frequency on the gas phase emitter effect of Dy16

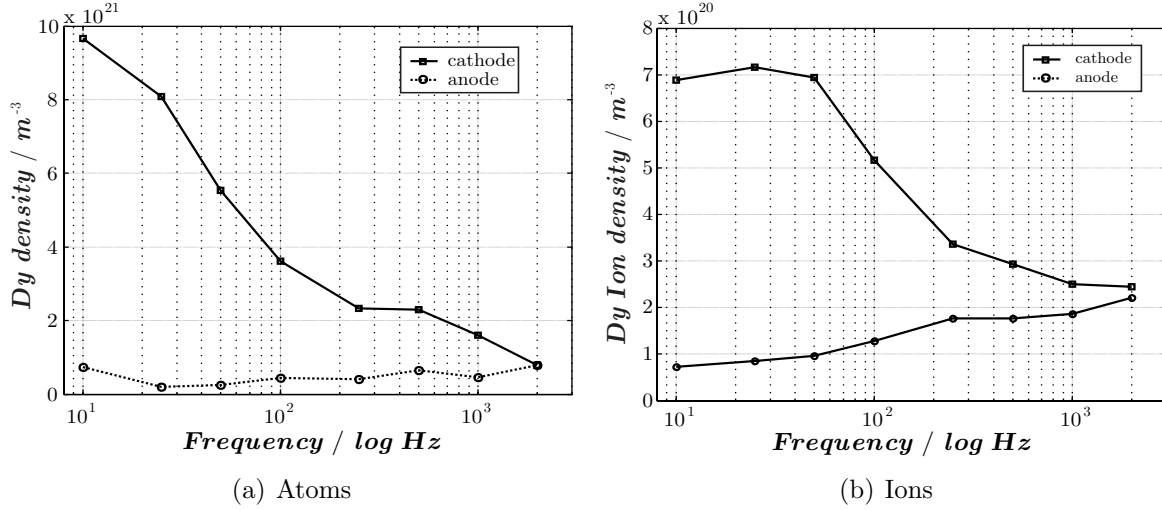


Figure 4. Maximum values of the Dy atom density $N_a(f)$ and Dy ion density $N_i(f)$ depending on frequency at a distance of $125 \mu\text{m}$ in front of the electrode. Parameter: DyI_3 , electrode diameter $d_E = 0.36 \text{ mm}$, electrode length $l_E = 5 \text{ mm}$, $i = 0.8 \text{ A}$ switched-dc

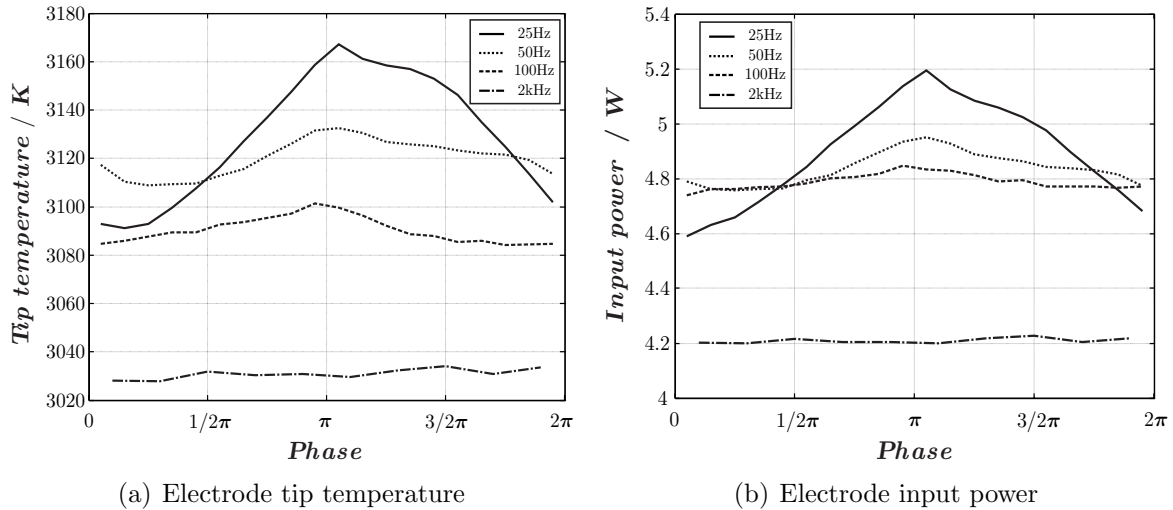


Figure 5. Electrode tip temperature $T_{tip}(\varphi)$ and input power $P_{in}(\varphi)$ over one period for various frequencies. Parameter: DyI_3 , electrode diameter $d_E = 0.36 \text{ mm}$, electrode length $l_E = 5 \text{ mm}$, $i = 0.8 \text{ A}$ switched-dc

phase but also within the cathodic phase is particularly noteworthy. This reduction within the cathodic phase differs from the weak increase observed in a pure argon or mercury atmosphere (figure 1(a)). Quite similar statements can be made if $P_{in}(\varphi)$ in figure 1(b) and figure 5(b) are compared. At $f = 2 \text{ kHz}$ the phase averaged power input P_{in} is reduced by approximately 30% compared to a lamp with a pure mercury filling.

Complementary the effect of different electrode diameters is investigated. For this

Investigating the influence of the operating frequency on the gas phase emitter effect of Dy17

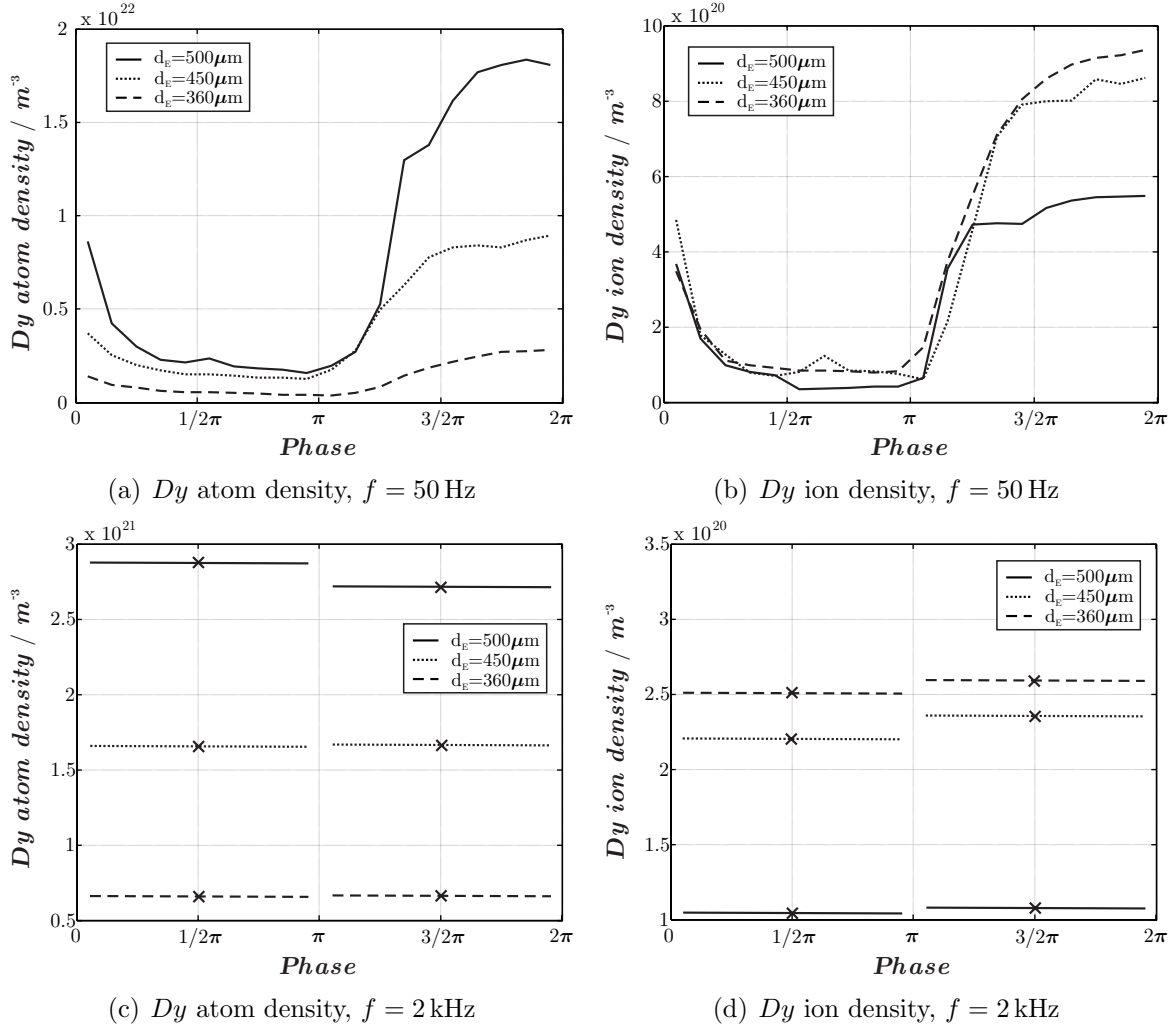


Figure 6. Dy atom density $N_a(\varphi)$ and ion density $N_i(\varphi)$ for frequencies of 50 Hz and 2 kHz over one period at a distance of 125 μm . Parameter: DyI_3 , electrode diameter $d_E = 0.36, 0.45$ and 0.5 mm , electrode length $l_E = 5 \text{ mm}$, $i = 0.8 \text{ A}$ switched-dc

purpose spectroscopic and pyrometric measurements are compared, being accomplished on lamps, which differ only by the electrode diameter. The different diameters are: $d_E = 360, 450$ and $500 \mu\text{m}$. The lamps are operated with a switched dc current of $i = 0.8 \text{ A}$ at operating frequencies of $f = 50 \text{ Hz}$ and 2 kHz . In figure 6 measurements of the densities of Dy atoms and Dy ions in front of the upper electrode are given. Figures 6(a) and 6(b) show $N_a(\varphi)$ and $N_i(\varphi)$, respectively, at $f = 50 \text{ Hz}$ for all three diameters. Within the cathodic phase distinctly higher densities of both Dy atoms and ions are found than within the anodic phase for all three electrode diameters. In the cathodic phase the density N_a becomes larger, N_i smaller with increasing electrode diameter. It corresponds to a decrease of the electron temperature within the boundary layer in front of the cathode with increasing electrode diameter at constant current according to [3], figure 6. Figure 6(c) and figure 6(d) represent only average values of N_a and

N_i within the anodic and cathodic half period for $f = 2$ kHz. For this high frequency the tolerable exposure time was too short and therefore the recorded number of counts too small for a more detailed phase resolution. Not only for $d_E = 360 \mu\text{m}$ but also for $d_E = 450, 500 \mu\text{m}$ a reduction of N_a within the cathodic phase towards the lower value within the anodic phase is observed. Also the ion densities N_i in both phases match at 2 kHz due to a lifting of N_i within the anodic phase and a lowering within the cathodic phase.

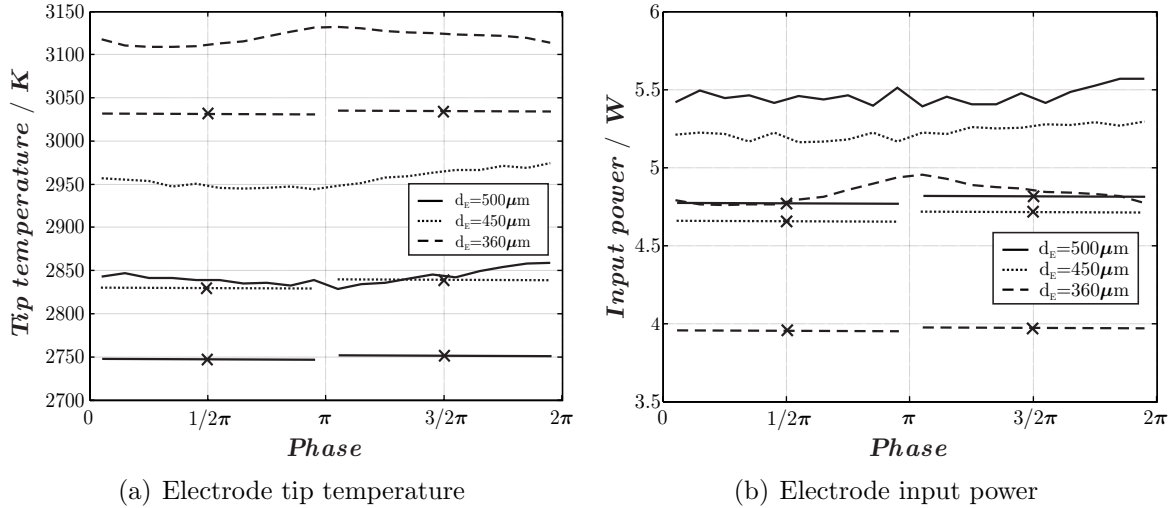


Figure 7. Electrode tip temperature $T_{tip}(\varphi)$ and input power $P_{in}(\varphi)$ for frequencies of 50 Hz (curves) and 2 kHz (crosses) over one period. Parameter: DyI_3 , electrode diameter $d_E = 0.36, 0.45$ and 0.5 mm, electrode length $l_E = 5$ mm, $i = 0.8$ A switched-dc

Comparing the particle densities in figure 3 and figure 6 for an electrode diameter $d_E = 360 \mu\text{m}$ it has to be taken into account that $N_a(\varphi)$ and $N_i(\varphi)$ are measured in different lamps of the same type. The differences are on the same order of magnitude as the measuring errors of $N_a(\varphi)$ and $N_i(\varphi)$ given in section 4.

In figure 7 T_{tip} and P_{in} are compared for the three electrode diameters. T_{tip} is lowered by an increase of d_E , the opposite applies for P_{in} . Both quantities are reduced by approximately the same amount for all three diameters, if the operating frequency is increased from 50 Hz to 2 kHz. The differences between T_{tip} and P_{in} for $d_E = 360 \mu\text{m}$ in figure 5 and figure 7 are negligible.

5.3. YAG lamp seeded with TlI and DyI_3

Previous measurements have suggested [16] that the emitter effect of dysprosium may be perturbed by other ingredients within the MH lamp. To substantiate this suspicion a YAG lamp was investigated, which was seeded with 1.242 mg DyI_3 and 0.758 mg TlI

Investigating the influence of the operating frequency on the gas phase emitter effect of Dy19

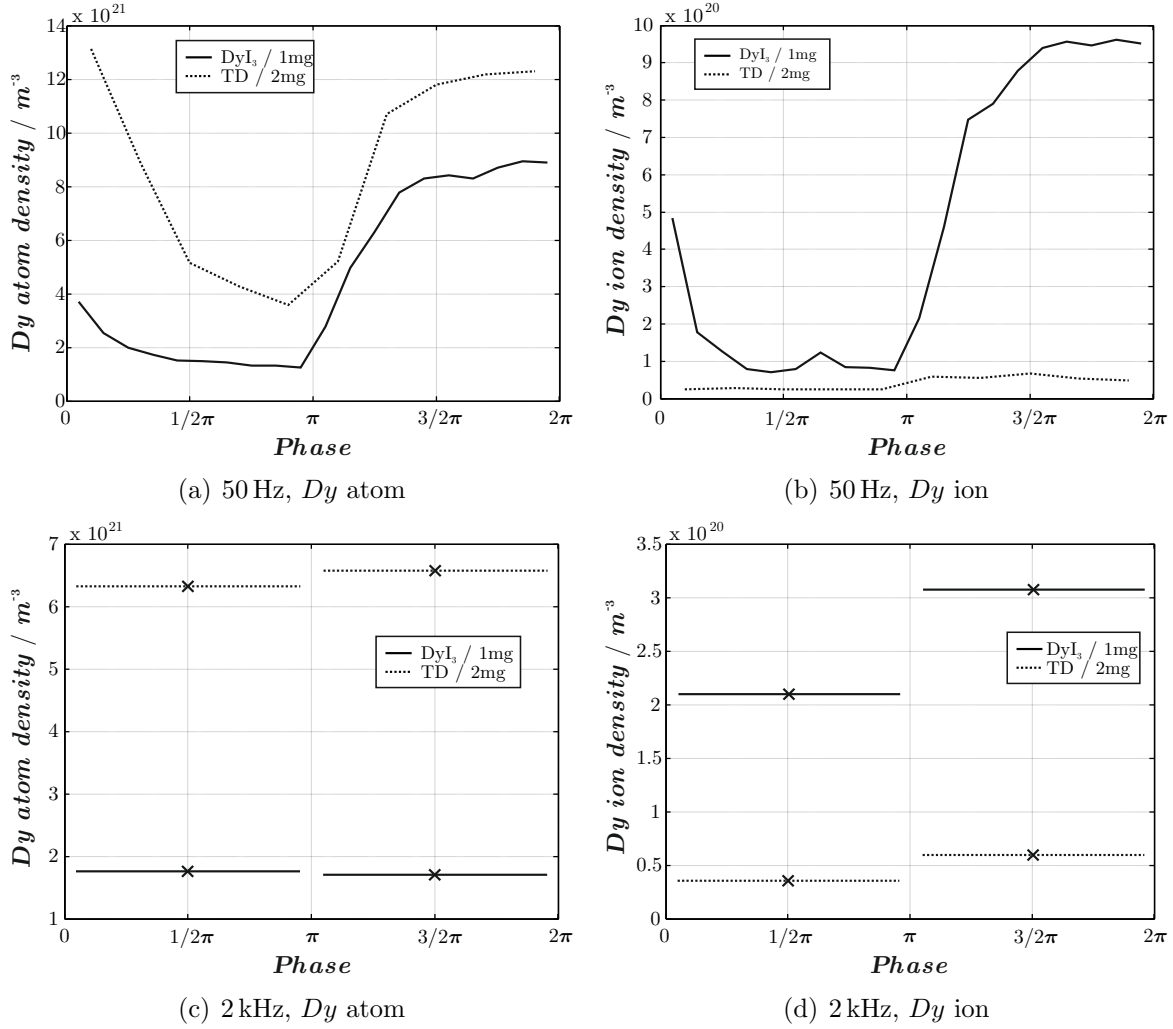


Figure 8. Phase resolved Dy atom density $N_a(\varphi)$ and ion density $N_i(\varphi)$ for a low and a high frequency (50 Hz and 2 kHz) for different lamp fillings. For the high frequency the values are average values over the anodic respectively cathodic phase. Parameter: DyI_3 , TD, electrode diameter $d_E = 0.45$ mm, electrode length $l_E = 5$ mm, $i = 0.8$ A switched-dc

(2 mg salt: 50 mol% DyI_3 and 50 mol% TlI , as mentioned in table 1). The results which were obtained with this so called TD-lamp are compared with those, which were obtained with the so called D-lamp. It was seeded as the lamps being investigated in section 5.2 with 1 mg DyI_3 . The electrode diameter was $d_E = 450 \mu\text{m}$. The lamps were operated with a switched dc current with an amplitude of $i = 0.8$ A being modulated with $f = 50$ Hz or $f = 2$ kHz. In figure 8 densities of Dy atoms and Dy ions are compared, which were measured in front of the upper electrode of the TD-lamp and D-lamp. Figure 8(a) and 8(b) represent the Dy atom density $N_a(\varphi)$ and the Dy ion density $N_i(\varphi)$, respectively, taken at an operating frequency of 50 Hz for the two lamps. For both lamps the Dy atom density N_a within the cathodic phase is much higher than within the anodic phase. It is even higher within the TD-lamp than within the D-lamp

corresponding to the higher amount of DyI_3 within the TD-lamp. The Dy ion density N_i in the TD-lamp is only marginally higher within the cathodic phase than within the anodic phase, in contrast to the D-lamp. Figure 8(c) and figure 8(d) give for $f = 2$ kHz only average values of N_a and N_i within the anodic and cathodic half period by the same reason as in figure 6(c) and 6(d). The density of the Dy atoms N_a within the cathodic phase is reduced to the level within the anodic phase while N_a within the anodic phase keeps the same value with increasing frequency. As in figure 8(a), N_a is higher within the TD-lamp than within the D-lamp. The density of the Dy ions N_i within the TD-lamp remains on the same low level as in figure 8(b). The variation of N_i within the D-lamp with increasing operating frequency was already discussed in section 5.2. In figure 9 courses of $T_{tip}(\varphi)$ measured within the TD-lamp and D-lamp are compared for the same operating conditions at $f = 50$ Hz and $f = 2$ kHz. Figure 9 clearly demonstrates that T_{tip} is nearly 300 K lower within the D-lamp than within the TD-lamp.

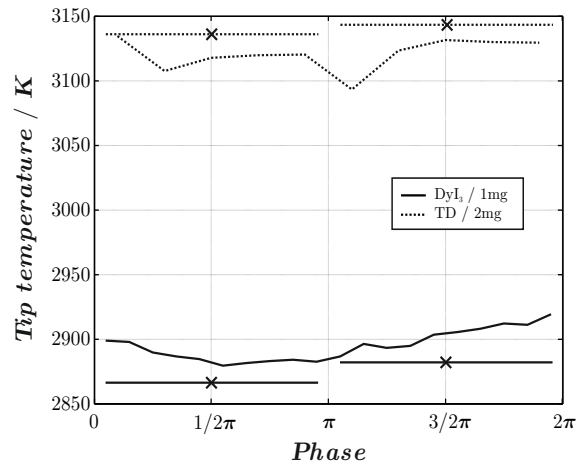


Figure 9. Phase resolved electrode tip temperature $T_{tip}(\varphi)$ for a low and a high frequency (50 Hz and 2 kHz) for different lamp fillings. For the high frequency the values are average values over the anodic and cathodic phase, respectively. Parameter: DyI_3 , TD, electrode diameter $d_E = 0.45$ mm, electrode length $l_E = 5$ mm, $i = 0.8$ A switched-dc

6. Interpretation of the measuring results

The particle density and electrode temperature measurements reveal a strong correlation between the Dy ion density in front of the electrode, and the electrode tip temperature and power input into the electrode. Compared to an equivalent pure mercury lamp operated with the same current $i(t)$ they are significantly lowered, if a high dysprosium ion density is measured in front of the electrode, as is demonstrated in figure 1, figure 3 and figure 5. A high Dy ion density is succeeded, with some time delay, by a high Dy atom density, as is illustrated in figure 3 and figure 6, but a high Dy atom density

is not accompanied in general by a high Dy ion density. An example of an exception is shown in figure 8. The Dy ion and atom density is generally higher within the cathodic half period than within the anodic half period independently of the operating frequency (figure 3), the electrode diameter (figure 6) and the composition of the lamp filling (figure 8). But with increasing operating frequency a decline of the Dy ion and atom density within the cathodic phase is observed together with a distinct increase of the Dy ion density within the anodic phase as is demonstrated in figure 4. Moreover a delayed adjustment of the Dy density on the electrode polarity can be observed especially at the beginning of the anodic phase, as shown in figure 6(a) and figure 6(b).

The accumulation of Dy ions and, with a time delay of several milliseconds, of Dy atoms in front of the cathode can only be explained by a cataphoretic transport of Dy ions from the bulk plasma to the electrode region within the cathodic phase. The related reduction of the electrode tip temperature has to be attributed to a lowering of the work function Φ of the cathode. It reduces the power loss of the cathode via thermionic electron emission, and with it the power transfer needed from the plasma to the cathode. The lowering of Φ is the effect of a Dy monolayer on the electrode surface. The growth and destruction of the monolayer depends on the adsorption/desorption energy of the Dy atoms on the tungsten surface, on the electrode tip temperature and the replacement rate of the desorbed Dy atoms from the gas phase. The measuring results are a strong indication that a Dy ion current plays a decisive role for the formation of a Dy monolayer within a MH lamp.

An emitter effect generated by an ion current should be limited to the cathode. Therefore, the reduction of the electrode temperature also within the anodic phase for operating frequencies on the order of 1 kHz has to be explained by a finite lifetime of the Dy -monolayer. If it is on the order of 1 ms, it will also reduce the work function Φ within the anodic phase for $f \geq 1$ kHz. The heating of the electrode within the anodic phase is approximately given by:

$$P_{in} \approx i \left(\Phi + \frac{5}{2} \frac{k_B T_{e,arc}}{e} \right), \quad (15)$$

where $T_{e,arc}$ is the average temperature of the electrons, which enter the constriction zone in front of the anode from the side of the bulk plasma. Therefore, a reduction of Φ diminishes the power input into the electrode not only within the cathodic phase but also within the anodic phase. It will explain the distinct reduction of T_{tip} at higher operating frequencies independently of the electrode diameter (figure 7).

The validity of eq. 15 at least for hot tungsten anodes is confirmed by measurements at the model lamp being analyzed in [10], section 5.2. The missing reduction of the power input into HID anodes operated with a dc current by doping them with ThO_2 [9, 10] does not provide an argument against the validity of eq. 15. Instead, it is

an indication that an emitter effect is generated by a thorium ion current towards the cathode, also in case of thoriated tungsten electrodes for HID lamps [35]. A publication of detailed investigations of the emitter effect at thoriated tungsten electrodes for HID lamps is under way. Eq. 9 in [36] and eq. 15, as well as the electron temperatures in these equations, are different since they apply to different situations. Eq. 9 in [36] is a theoretical expression for the power flux density from the plasma sheath immediately in front of the electrode while eq. 15 describes the power transfer from the anodic boundary layer composed of the plasma sheath and the constriction zone to the anode.

The effect of an additional seeding of the YAG lamp with *TlI* is demonstrated in figure 8 and figure 9. The thallium additive inhibits the formation of *Dy* ions in front of the cathode as is shown by the measuring results in figure 8. The ionisation energy of *Tl*, $E_i = 6.11$ eV, exceeds that of *Dy* only by 0.19 eV so that the ionisation degree of *Tl* may be comparable with that of *Dy*. But the vapour pressure of *Tl* is distinctly higher than that of *Dy*. Assuming a cold spot temperature T_{csp} of the YAG lamp in the 1150 – 1200 k range the corresponding pressure ratio $p(Tl)/p(Dy)$ amounts to 350 and 90, respectively [37]. The low values of the *Dy* ion density $N_i(\varphi)$ are reflected by a high electrode tip temperature T_{tip} in figure 9. Further investigations into the TD-lamp are needed to clarify the reduction of the *Dy* ion density but not of the *Dy* atom density in front of the cathode. An interpretation of the result is difficult, since the *Dy* atoms are accumulated by the cataphoretic transport of *Dy* ions in front of the cathode.

Another very common ingredient of MH lamps is sodium. Measuring results given in [16] raise suspicion that *Na* ions displace *Dy* ions in front of the cathode so that the formation of a *Dy* monolayer on the electrode surface is hampered. The effect of *Na* and of a salt mixture consisting of *NaI*, *TlI* and *DyI₃* on the electrode properties in MH lamps will be investigated in detail separately.

Measurements given in [29] indicate that the current wave form has a considerable influence on the gas phase emitter effect. Lower average electrode temperatures were found with a sinusoidal current than with a switched dc current of the same effective value. The influence of the different current wave forms will be investigated in detail in a subsequent paper.

7. Concluding remarks

The measurements at a YAG lamp seeded with *DyI₃* confirm the initial speculation that a reduction of the work function by a gas phase emitter effect within the cathodic half period may overlap onto the anodic half period at higher operating frequencies. The condition is a sufficiently high lifetime of the atomic monolayer being formed by the emitter material. The lifetime depends among others on the intensity of the cataphoretic transport of ionized emitter material towards the cathode, the adsorption/desorption

energy of the emitter atoms on the electrode surface and the temperature of the electrode surface. The cataphoretic transport of emitter material is in addition sensitively dependent on the gas composition as the example of a seeding with DyI_3 and TII has shown. Therefore it may be a difficult task to optimize the emitter effect in commercial MH lamps seeded by a mixture of metal iodides.

8. Acknowledgements

The authors thank Philips Lighting, NL, for scientific and financial support. Financial support from Deutsche Forschungsgemeinschaft (Graduiertenkolleg 1051) and from the Research School of the Ruhr-University of Bochum is also gratefully acknowledged by the authors.

References

- [1] Lichtenberg S *et al* 2002 *J. Phys. D: Appl. Phys.* **35** 1648-1656
- [2] Lichtenberg S *et al* 2005 *J. Phys. D: Appl. Phys.* **38** 3112-3127
- [3] Dabringhausen L *et al* 2005 *J. Phys. D: Appl. Phys.* **38** 3128-3142
- [4] Benilov M S *et al* 2002 *J. Phys. D: Appl. Phys.* **35** 1-15
- [5] Waymouth J F 1971 *Electric Discharge Lamps, Monographs in Modern Electrical Technology* (Cambridge, MA: MIT Press)
- [6] Dabringhausen L *et al* 2002 *J. Phys. D: Appl. Phys.* **35** 1621-1630
- [7] Luhmann J *et al* 2002 *J. Phys. D: Appl. Phys.* **35** 1631-1638
- [8] Nandelstaedt D *et al* 2002 *J. Phys. D: Appl. Phys.* **35** 1639-1647
- [9] Redwitz M *et al* 2006 *J. Phys. D: Appl. Phys.* **39** 2160-2179
- [10] Mentel J and Heberlein J 2010 *J. Phys. D: Appl. Phys.* **43** 023002
- [11] Westermeier M *et al* 2010 *J. Phys. D: Appl. Phys.* **43** 124015
- [12] Luijks G M J F *et al* 2005 *J. Phys. D: Appl. Phys.* **38** 3163-3169
- [13] Almanstoetter J *et al* 2002 *J. Phys. D: Appl. Phys.* **35** 1751-1756
- [14] Hartmann T *et al* 2010 *J. Phys. D: Appl. Phys.* **43** 025201
- [15] Tielemans P and Oostvogels F 1983 *Philips J. Res.* **38** 214-223
- [16] Langenscheidt O *et al* 2008 *J. Phys. D: Appl. Phys.* **41** 144005
- [17] Luijks G M J F *et al* 2008 *J. Phys. D: Appl. Phys.* **41** 144006
- [18] Miedema A R and Dorleijn J W F 1980 *Surface Science* **95** 447-464
- [19] Medvedev B K, Ionov N I and Belyakov Yu I 1974 *Sov. Phys. Solid State* **15** (9) 1743-1746
- [20] Alekseev N I 1968 *Soviet Physics - Technical Physics* **12** (12) 1639-1642
- [21] Westermeier M *et al* 2008 *IEEE Transactions on Plasma Science* **36** (4) 1176-1177
- [22] Hartmann T *et al* 2002 *J. Phys. D: Appl. Phys.* **35** 1657-1667
- [23] Redwitz M *et al* 2005 *J. Phys. D: Appl. Phys.* **38** 3143-3154
- [24] Langenscheidt O *et al* 2007 *J. Phys. D: Appl. Phys.* **40** 415-431
- [25] Reinelt J *et al* 2008 *J. Phys. D: Appl. Phys.* **41** 144002
- [26] Benilov M S 2008 *J. Phys. D: Appl. Phys.* **41** 144001
- [27] Benilov M S *et al* 2005 *J. Phys. D: Appl. Phys.* **38** 3155-62
- [28] Reinelt J *et al* 2011 *J. Phys. D: Appl. Phys.* **44** 095204
- [29] Reinelt J 2009 *Experimental investigation on electrodes of HID lamps at low and high operating frequencies PhD thesis, Ruhr University Bochum*
- [30] Dabringhausen L 2004 *Charakterisierung von Elektroden für Hochdruck-Plasmalampen durch Pyrometrie und Simulation PhD thesis (Berlin Tenea) Ruhr Universität Bochum*

Investigating the influence of the operating frequency on the gas phase emitter effect of Dy24

- [31] DeVos J C 1954 *Physica* **20** 690-714
- [32] Westermeier M *et al* 2010 *Phase resolved Dy-density and plasma temperature measurements by absorption- and emission-spectroscopy of Dy spectral lines*, *Proc. 12th Int. Symp. on the Science and Technology of Light Sources and the 3rd Int. Conf. on White LEDs and Solid State Lighting (Eindhoven (NL), 11-16 July 2010)* ed Haverlag M *et al* CP060, 165-166
- [33] Schoepp H 2002 *Elektrische und strahlungsphysikalische Eigenschaften von Hochdruckentladungen - insbesondere Quecksilberdampfentladungen - für die Beleuchtungstechnik (Berlin: Technische Universität)*
- [34] Kurucz R *et al* 1995 KURUCZ CD-ROM NO. 23 - *Atomic Line List (Cambridge, MA: Harvard-Smithsonian Center for Astrophysics)*
- [35] Bergner A *et al* 2010 *Temperature measurements at thoriated cathodes in a model lamp and its interpretation by numerical simulation*, *Proc. 12th Int. Symp. on the Science and Technology of Light Sources and the 3rd Int. Conf. on White LEDs and Solid State Lighting (Eindhoven (NL), 11-16 July 2010)* ed Haverlag M *et al* CP128, 373-374
- [36] Almeida N A *et al* 2009 *J. Phys. D: Appl. Phys.* **42** 045210
- [37] Welters W *Philips Lighting, GBU HID, P.O.box 80020, 5600JM Eindhoven, The Netherlands*
private communication